CHAPTER 5

HOMODINUCLEAR TRI, [ONO]- AND TETRADENTATE, $[N_2O_2]$-DONOR SCHIFF BASE COMPLEXES OF COPPER(II) AND ZINC(II)

CHAPTER 5

HOMODINUCLEAR TRI, [ONO]- AND TETRADENTATE, $[N_2O_2]$-DONOR SCHIFF BASE COMPLEXES OF COPPER(II) AND ZINC(II)

5.1 Introduction:

The design, synthesis and structural characterization of Schiff base metallomesogens has received tremendous impetus during the last few decades owing to versatile physico-chemical properties (colour, magnetism, polarisability, redox behaviour etc.) of such metal-organic frameworks.[1-6] A considerable effort is being invested in the development of new chelating ligands; particularly, the versatile binucleating imino ligands which exhibit very rich coordination chemistry, such species occupy an important position in modern inorganic chemistry.[7-9] Numerous examples of mononuclear metallomesogens exhibiting novel mesomorphic properties have been widely reported, examples of bi-metallomesogens are still quite rare.[10-18] The design of binuclear metallomesogens thus constitutes a key step for the development of magnetic and conductive materials.[16,18,19] Among the documented bimetallic mesogens, majority is diamagnetic.[20-22] Paramagnetism induced by a metal centre can lead to interesting chemical and physical properties.[23-26] Lai and Leu[10] reported a series of oxygen-bridged bimetallomesogens containing copper(II), palladium(II), oxovanadium(IV) and iron(II) ions based on salicylaldimines ligands, namely, N-(3-hydroxypropyl)-4-alkoxysalicylaldimines and N-(3-hydroxypropyl)-4-(4-alkoxybenzoyl)salicylaldimines. Luminescent liquid crystalline materials have attracted increasing attention as well owing to their versatile exploration of display devices, solar cells, information storage system and sensors.[27-29] Besides the well-known display applications of luminescent liquid crystals (LCs), their synthesis is still challenging. Most of the molecular emitters are highly emissive in solution and in solid states; however, luminescent properties in the mesomorphic states are quite rare.[30-32] Since the discovery and advancement of light-emitting devices, zinc complexes have received significant attention because of their interesting

photoluminescent properties, high thermal, redox stability and great diversity of tunable electronic properties.[6,33-36] In this chapter we report series of bimetallic Cu(II)/Zn(II) complexes accessed from new binucleating Schiff bases with tridentate[NOO]-donor and compartmental tetradentate[N_2O_2]-donor ligand with an aromatic/alcohol amine rigid spacer and 4-substituted long/short alkoxy group at the side.

5.2 Experimental:

5.2.1 Synthesis of dinuclear zinc complexes bearing tetradentate [N_2O_2] donor of Schiff base ligands:

Synthesis of salicylaldimine ligands condensed from 3′, 3′, 4′, 4′-tetraminobiphenyl and 4-substituted long/short alkoxy salicylaldehyde possessing two set of tetradentate [N_2O_2] donor site and their binuclear zinc(II) complexes have been presented in **scheme 1**.

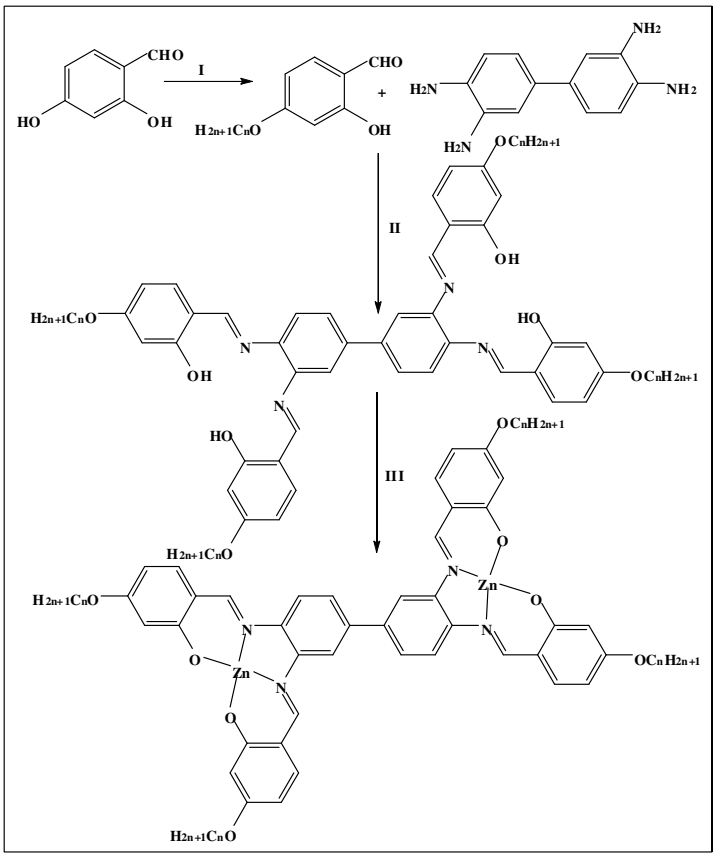

Scheme 1: i.$C_nH_{2n+1}Br$, $KHCO_3$, KI, dry acetone, Δ, 40h, and ii. glacial AcOH, absolute EtOH Δ, 4h iii. $Zn(OAc)_2.2H_2O$, MeOH, TEA. Δ, 1h.

Synthesis of n-alkoxysalicyldehydes (n = 6, 12):

Alkoxysalicyldehyde derivatives were prepared following a reported method.[37,38] 2, 4-Dihydroxybenzaldehyde (10mmol, 1.38g), $KHCO_3$ (10mmol, 1g), KI (catalytic amount) and 1-bromohexane (10mmol, 1.6g) or 1-bromododacane (10mmol, 2.4g) were mixed in 250 mL of dry acetone. The mixture was heated under reflux for 24 h, and then filtered, while hot, to remove any insoluble solids. Dilute HCl was added to neutralize the warm solution, which was then extracted with chloroform (100mL). The combined chloroform extract was concentrated to give a purple solid. The solid was purified by column chromatography using a mixture of chloroform and hexane (v/v, 1/1) as eluent. Evaporation of the solvents afforded a white solid product.

Synthesis of Schiff base ligand (6bps):

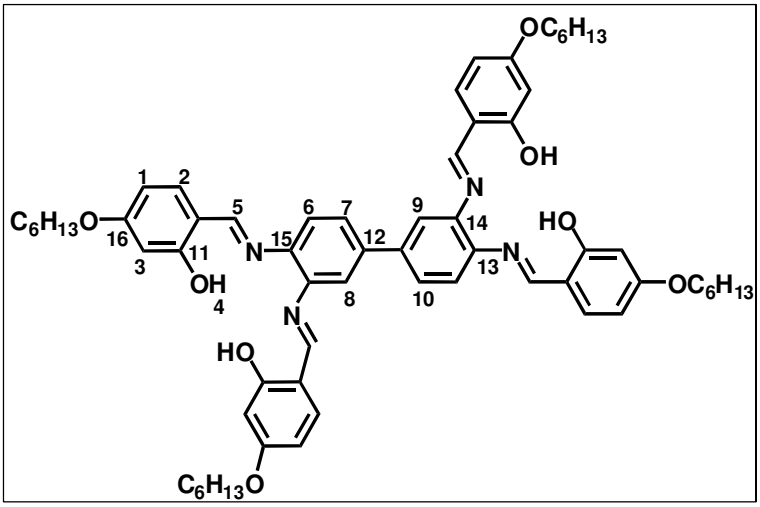

An ethanolic solution of 2-hydroxy-(4-hexyloxy)- salicyldehyde (0.88g, 4mmol) or 2-hydroxy-(4-hexyloxy)-salicyldehyde (1.22g, 4mmol) was added to an ethanolic solution of 3′,3′,4′,4′-tetraminobiphenyl (0.21g, 1mmol).The solution mixture was refluxed with a few drops of acetic acid as catalyst for 3h to yield the yellow Schiff base. The compound was collected by filtration and recrystallised from absolute ethanol to obtain a pure compound.Yield:0.81g (75%). m.p.133°C. Anal. Calc. for $C_{64}H_{78}N_4O_8$: C, 74.5; H, 7.6; N, 5.4. Found: C, 74.7; H, 7.8; N, 5.3%; FAB Mass (m/e, fragment): m/z: calc. 1030.5; found: 1031[$M+H^+$]; ^{1}H NMR (400 MHz, $CDCl_3$): δ = 13.07 (s, 1H, H^4), 8.51 (s, 1H, H^5), 7.14 (t, J = 8.43 Hz, 2H, H^2), 6.54 (d, J = 2.44 Hz, 2H, H^3), 6.49 (dd, J = 2.44 Hz, J = 8.29 Hz, 2H, H^2), 3.97 (t, J = 6.8 Hz, 2H, -OCH_2), 0.89 (t, J=6.8Hz, 6H, CH_3). ^{13}C NMR (75.45 MHz; $CDCl_3$; Me_4Si at 25°C,

ppm), δ = 107.5(-C1), 130.7(-C2), 160.9(-C16), 160.6(-C5), 122.4(-C8), 161.6(-C11), 144.4(-C15), 121.8(-C9), 135.7(-C12). IR ($\nu_{max,\ cm}^{-1}$, KBr): 3500 (ν_{OH}), 2925 ($\nu_{as(C-H),}CH_3$), 2921 ($\nu_{as(C-H),}CH_2$), 2873 ($\nu_{s(C-H),}CH_3$), 2850 ($\nu_{as(C-H),}CH_2$), 1629 ($\nu_{C=N}$), 1298 (ν_{C-O}).

Synthesis of Schiff base ligand (12bps):

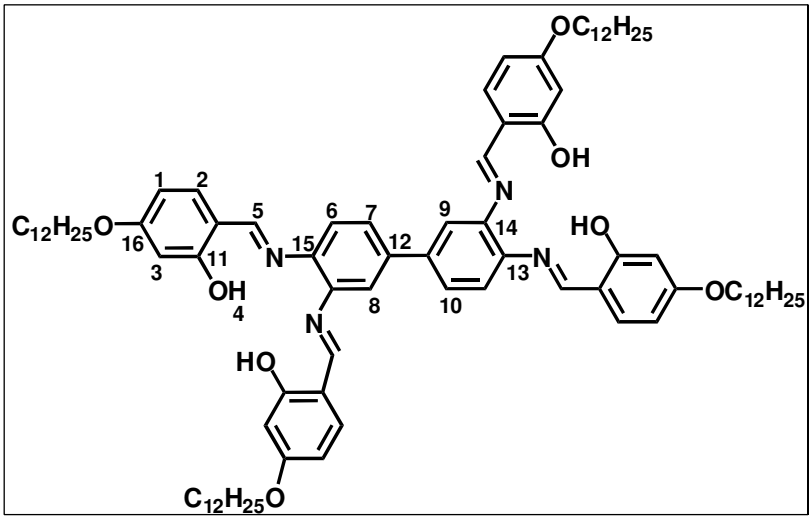

Yield: 1.08g (76%). m.p., 117°C. Anal. Calc. for $C_{88}H_{126}N_4O_8$: C, 77.2; H, 9.2; N, 4.1. Found: C, 77.1; H, 9.1; N, 4.2%; FAB Mass (m/e, fragment): m/z: calc. 1366.9; found: 1367[M+H$^+$]; ^{1}H NMR (400 MHz, $CDCl_3$): δ = 13.06 (s, 1H, H^4), 8.55 (s, 1H, H^5), 7.13 (t, J = 8.42Hz, 2H, H^2), 6.53 (d, J = 2.43 Hz, 2H, H^3), 6.48 (dd, J = 2.44 Hz, J = 8.27 Hz, 2H, H^2), 3.99 (t, J = 6.8 Hz, 2H, -OCH_2), 0.88 (t, J=6.8Hz, 6H, CH_3). ^{13}C NMR(75.45 MHz; $CDCl_3$; Me_4Si at 25°C, ppm), δ = 106.5(-C1), 130.8(-C2), 161.9(-C16), 162.6(-C5), 122.4(-C8), 161.6(-C11), 143.4(-C15), 121.7(-C9), 135.6(-C12). IR ($\nu_{max,\ cm}^{-1}$, KBr): 3500 (ν_{OH}), 2924 ($\nu_{as(C-H),}CH_3$), 2922 ($\nu_{as(C-H),}CH_2$), 2874($\nu_{s(C-H),}CH_3$), 2851 ($\nu_{as(C-H),}CH_2$), 1628 ($\nu_{C=N}$),1297 (ν_{C-O}).

Synthesis of dinuclear zinc(II) complex (Zn_2-6bps.):

The ligand 6bps (0.051g, 0.05mmol) or 12bps (0.068g, 0.05mmol) was dissolved in minimum volume of absolute ethanol. To this, an equimolar amount of zinc acetate $Zn(OAc)_2.2H_2O$ (0.02g, 0.1mmol) in methanol was then added slowly and stirred for 2h at room temperature. A brown solid formed was filtered, washed with diethyl ether and finally with chloroform-ethanol (1:1).

Yield: 0.05g (75%). m.p., 318°C. Anal. Calc. for $C_{64}H_{74}Zn_2N_4O_8$: C, 66.3; H, 6.4; N, 4.8. Found: C, 66.5; H, 6.3; N, 4.8%; FAB Mass (m/e, fragment): m/z: calc. 1156.4; found: 1157[$M+H^+$]; ^{1}H NMR (400 MHz, $CDCl_3$): 8.54 (s, 1H, H^5), 7.11 (t, J = 8.38 Hz, 2H, H^2), 6.51 (d, J = 2.39 Hz, 2H, H^3), 6.47 (dd, J = 2.44 Hz, J = 8.29 Hz, 2H, H^2), 3.91 (t, J = 6.8 Hz, 2H, -OCH_2), 0.87 (t, J=6.8Hz, 6H, CH_3). IR ($\nu_{max,\ cm}^{-1}$, KBr): 2924 ($\nu_{as(C-H),}CH_3$), 2922 ($\nu_{as(C-H),}\ CH_2$), 2871 ($\nu_{s(C-H),}CH_3$), 2849 ($\nu_{as(C-H),}\ CH_2$), 1614 ($\nu_{C=N}$), 1296 (ν_{C-O}).

Complex Zn_2-12bps:

Yield: 0.06g (78%). m.p., 312°C. Anal. Calc. for $C_{88}H_{122}Zn_2N_4O_8$: C, 70.7; H, 8.2; N, 3.7. Found: C, 70.5; H, 8.3; N, 3.8%; FAB Mass (m/e, fragment): m/z: calc. 1493.7; found: 1494[$M+H^+$]; ^{1}H NMR (400 MHz, $CDCl_3$): 8.57 (s, 1H, H^5), 7.12 (t, J = 8.37 Hz, 2H, H^2), 6.54 (d, J = 2.38 Hz, 2H, H^3), 6.48 (dd, J = 2.45 Hz, J = 8.28 Hz, 2H, H^2), 3.92 (t, J = 6.7 Hz, 2H, -OCH_2), 0.88 (t, J=6.7Hz, 6H, CH_3). IR ($\nu_{max,\ cm}^{-1}$, KBr): 2923 ($\nu_{as(C-H),}CH_3$), 2922 ($\nu_{as(C-H),}\ CH_2$), 2871 ($\nu_{s(C-H),}CH_3$), 2848 ($\nu_{as(C-H),}\ CH_2$), 1611 ($\nu_{C=N}$), 1295 (ν_{C-O}).

5.2.1.1 Results and discussion:

Synthesis and structural assessment:

The synthetic procedure for ligands and metal complexes are depicted in Scheme 1. The Schiff base ligands were synthesized by literature procedures[37,38] and were identified by ^{1}H NMR, ^{13}C NMR and elemental analysis. The compounds were obtained as yellow microcrystalline solids in good yields. The bimetallic zinc(II) complexes, prepared by reacting the appropriate tetraimine with zinc(II) acetate dihydrate in methanol, was isolated as a brown solid in good yield. The complexes were soluble in chloroform and dichloromethane and insoluble in ethanol. The CHN microanalyses of the Schiff base ligands and the zinc complexes are consistent with the proposed formulas, confirming the bimetallic composition of the complex. The FAB-mass spectra of the compounds matched well with their formula weights. The IR spectrum of the Schiff base ligand showed a broad band in the region 3480-3466cm^{-1} attesting the presence of OH group. The band disappears upon complexation. The azomethine nitrogen $\nu_{C=N}$ stretching frequency of the free ligand appears at ~1629cm^{-1}, that shifted to lower wave numbers in the spectrum of the complexes

(~1614cm^{-1}), indicating the involvement of azomethine nitrogen in coordination. The ligand with four terminal chains around, serve as a chelating agent with two set of tetradentate [N_2O_2] core each set comprising of two phenolate-oxygen and two azomethine nitrogen atoms (**Scheme 1**). Appearance of medium intensity bands at 480-450cm^{-1} attributable to ν_{M-N} and ν_{M-O} respectively. ^{1}H NMR spectra of ligands show signal at δ 13.4-13.8ppm, corresponding to the proton of the OH group. The proton NMR signal of the imine group appears at δ 8.5ppm for ligand. Absence of the phenolic –OH proton and a downfield shift in the peak positions of the –N=CH proton in the ^{1}H NMR spectrum of the metal complex further suggest binding through the phenolate oxygen and the azomethine nitrogen atoms of the ligand to the metal ion.[6, 37,38] Solution electrical conductivity of complexes recorded in CH_2Cl_2 (10^{-3}M) were found to be < 10 $\Omega^{-1}cm^{-1}mol^{-1}$, much lower than is expected for a 1:1 electrolyte, thus confirming the non-electrolytic nature of the complex.[39,40]

Photophysical properties:

The UV-vis absorption spectrum (**Fig.1**) of free ligand consists of an intense band centered at ~399 nm attributed to π-π* transitions of the azomethine group. Another intense band (~333 nm) in the higher energy region was related to π-π* transitions of benzene rings. These transitions shifted to lower wave numbers in the complexes. A shoulder at ~ 488 nm has been assigned to MLCT transition.

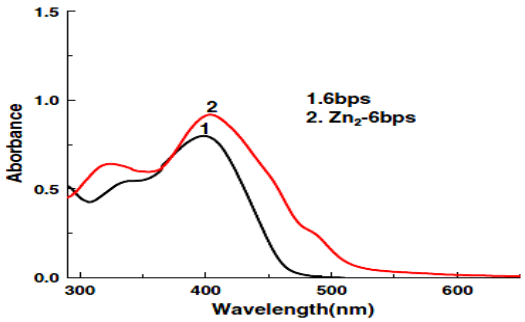

Fig. 1: UV-visible spectra of 6-bs and Zn_2-6bps.

Photoluminescence study of the ligands and zinc(II) complexes were carried out at room temperature in dichloromethane solution and also in the solid state (**Fig.2** and **Fig.3**). The ligands emit green light both in solution as well as in the solid state at 512nm (Φ = 30%) and 549nm (Φ = 16%), respectively, when excited at 330nm. The solid state emission spectrum of the complexes was recorded by placing a uniform

powder sheet between two quartz plates. Generally Schiff base systems exhibit florescence due to intraligand π-π* transitions.[41] Quite surprisingly, upon complexation, the emission maxima is shifted to higher energy (λ_{max} = 452nm, Φ = 20%) resulting in blue light emission. This is not usual, as one would expect the emission band of the free ligand to be at higher energy related to that of the complex because of its relatively high-energy excitation band. This anomaly can be explained by the fact that excited states originating from complexes of Zn^{2+} are typically ligand-centered in nature owing to the inability of the d^{10} metal center to participate in low-energy charge transfer for metal-centered transitions.[42-44] However, in solid state the complexes emit green light at ~555nm (Φ = 11%). In solid state after complexation, the free rotation of the flexible bonds of the ligand is reduced and hence energy dissipation through non-radiative channels decreases leading to shift of emission wave length to lower energy. The intense emission observed at room temperature in the complex stems from the intraligand (π-π*) fluorescence, and the role of the Zn^{2+} ion is to provide stability to the ligand.[45] The spectral data of all the compounds are shown in the Table 1.

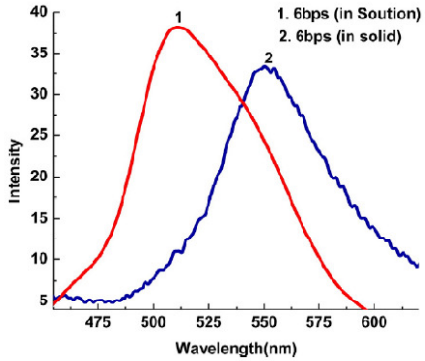

Fig. 2: Emission spectrum of 6-bps in solution and in solid state.

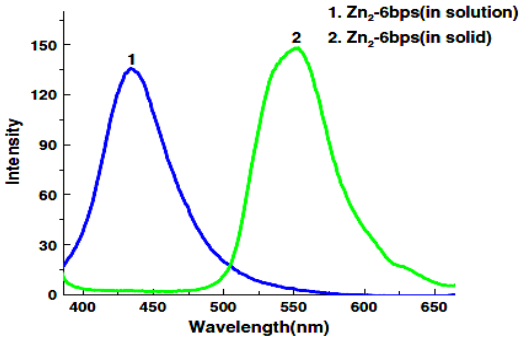

Fig. 3: Emission spectrum of Zn_2-6bps in solution and in solid state.

Table 1: UV-visible and photoluminescence data of ligands (n-bps) and Zn_2-nbps Complexes.

Compounds	π→π* (ε, l mol^{-1} cm^{-1})	π→π* (ε, l mol^{-1} cm^{-1})	MLCT(ε, l mol^{-1} cm^{-1})	PL[a] (Solution)	PL[a] (Solid)
6bps	335 (5300)	399(9800)	-	512	549
Zn_2-bps	323 (11200)	398(9100)	488(2200)	452	555
12bps	330(5200)	399(9700)	-	516	554
Zn_2-bps	316 (5400)	396(8200)	488(2300)	451	558

[a] Photoluminescence data of compounds.

Mesomorphic behaviour: Polarising Optical Microscopy (POM) and Differential Scanning Calorimetry (DSC) studies:

Hot-stage polarizing optical microscopy has been used to study the interference patterns of the birefringent liquid crystalline materials. Characteristic textures associated with different mesophases were identified by comparison with those reported in the literature. The ligand, 6bps exhibited monotropic liquid crystalline behavior. On slow cooling from the isotropic liquid, the compound showed a birefringent schlieren texture (**Fig.4**) typical of a nematic mesophase at ~128°C. DSC study (Table 2) showed two transitions in heating run and one in the cooling run (**Fig.5**). The transition at 133.7°C (ΔH = 13.2kJmol^{-1}) is due to the N-I transition. Isotropic to nematic transition could not be detected in DSC, probably due to slow crystallization or vitrification of the mesophases. Owing to the high viscous nature of the 6bps compound, transition peaks observed in DSC were rather broad. Quite interestingly, the long chain compound 12-bps showed enantiotropic SmC phase with four brush defect (**Fig. 6**). The DSC thermogram exhibited two sharp transitions in heating and two in cooling cycle (**Fig. 7**). The marked difference in the mesomorphic behaviour of 6bps and12bps due to the presence of short (C_6) and long (C_{12}) alkoxy chain is noteworthy. We are, however, unable to provide any suitable explanation at this moment. Increased alkoxy chain length might have affected the overall orientation of the molecule including the torsional twist of the biphenyl rings which in turn modified the intermolecular association. Pertinent here is to mention that somewhat similar biphenyl based compartmental Schiff base ligands with ester linkages showed smectic mesomorphism.[16] Most of other related compartmental Schiff base ligands were documented with no reported mesogenicity.[46] Owing to the high viscous nature of the compound (6bps) transition peaks observed in DSC were rather broad. Upon coordination to zinc(II) the mesogenic property of the Schiff base ligands were completely lost. Desired molecular shape to enhance anisotropy in intermolecular forces is often not possible to achieve for chemical feasibility reasons. Thus unfavourable structural orientation of the resulting binuclear complex molecules is believed to have upset the mesogenicity in the present case. Similar loss of mesomorphism was earlier reported for related binuclear Schiff base metal complexes of copper (II) and nickel (II).[47]

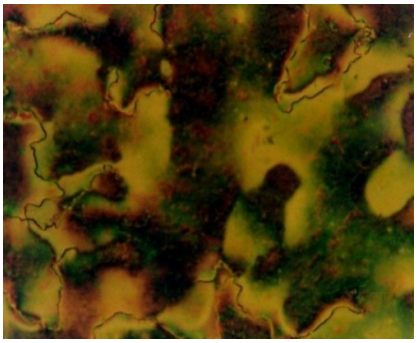

Fig. 4: Schlieren texture of nematic phase of 6bps at 128°C.

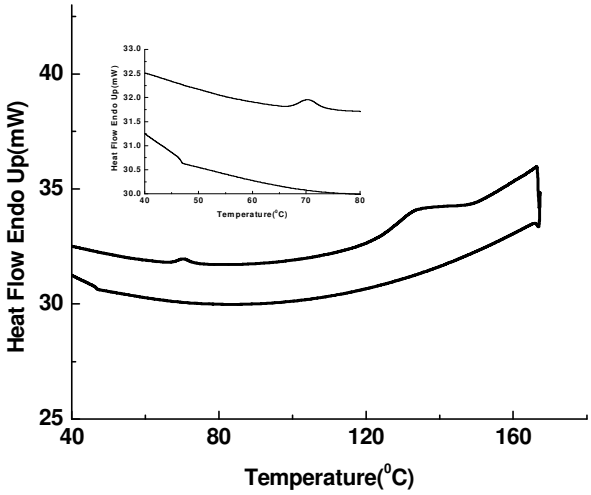

Fig. 5: DSC thermogram of 6bps.

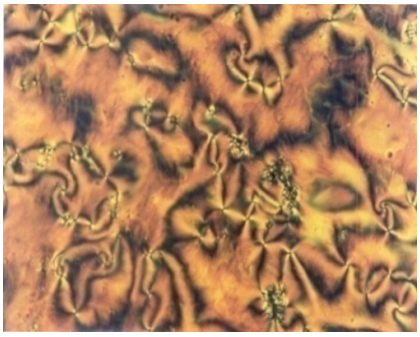

Fig. 6: Schlieren texture of SmC of 12bps at 117°C.

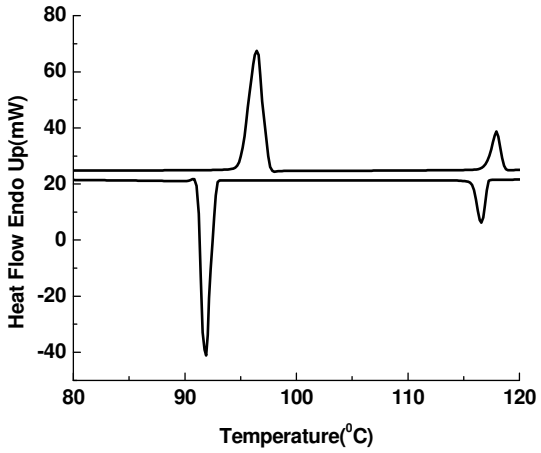

Fig. 7: DSC thermogram of (12bps).

Table 2: DSC data of the complexes.

Compounds	**T [°C][a]**	**Transition[b]**	**ΔH [kJmol^{-1}]**
6bps	70.3	Cr-N	1.3
	133.7	N-I	13.2
	47.2	I-Cr	0.79
12bps	96.5	Cr-SmC	74.4
	117.8	SmC-I	14.6
	116.1	I-SmC	13.8
	91.7	SmC-Cr	74.1

[a] Transition temperature obtained from onset peak.

[b] Cr: crystal; N: Nematic phase; SmC: Smectic phase; I: Isotropic phase.

DFT study:

As a representative case, the ground state geometries in the gas phase of the ligand molecule (6bps) and its zinc complex, Zn_2-6bps (**Fig. 8**) were fully optimized using the restricted BLYP/DNP methods without imposing any symmetry constrain. The BLYP functional used throughout this study, comprises of a hybrid exchange functional as defined by Becke and the non-local Lee–Yang–Parr correlation functional.[48] The basis set chosen in this study is DNP, the double-numerical atomic orbitals augmented by polarization functions. All calculations were performed with the DMol3 program package.[49-51] In our calculations, self consistent field procedures

are performed with a convergence criterion of 2×10^{-5} a.u. on the total energy and 10^{-6} a.u. on electron density. The 3D isosurface plots of the lowest unoccupied molecular orbital (LUMO) and the highest occupied molecular orbital (HOMO) of the complex are shown in (**Fig.9** and **Fig.10**). The HOMO and LUMO energies of the ligand are calculated to be -4.70eV and -2.49eV, respectively, ΔE = 2.21eV. The corresponding energies of the Zn-complex found to be -4.74eV, -2.76eV and ΔE = 1.98eV, respectively, matched well with those reported for similar Schiff base complexes of zinc.[16,38] The HOMO-LUMO energy difference decreases substantially on incorporation of two zinc ions into the ligand framework. The HOMO–LUMO energy separation can be related to kinetic stability and in turn reactivity pattern of the molecule. A small HOMO–LUMO gap implies a low kinetic stability and high chemical reactivity, because it is energetically favourable to add electrons to LUMO or to extract electrons from a HOMO. Selective geometric parameters of the optimized zinc complex were evaluated by DFT at BLYP/DNP level (Table 3).The complex has an average Zn—O and Zn—N bond lengths 1.97 and 2.10Å, respectively. The average bond angles 97.6° and 79.3° for O1–Zn–O2 and N1–Zn–N2, respectively, around the zinc atom which deviates substantially from the tetrahedral values indicated a distorted planar four coordinate geometry. These geometrical parameters match well with structurally characterized analogous zinc complexes.[41,50] Biphenyl, a short rigid central bridge presumably prevented the formation of a tetrahedral environment around zinc (II), leading to a distorted square planar geometry.

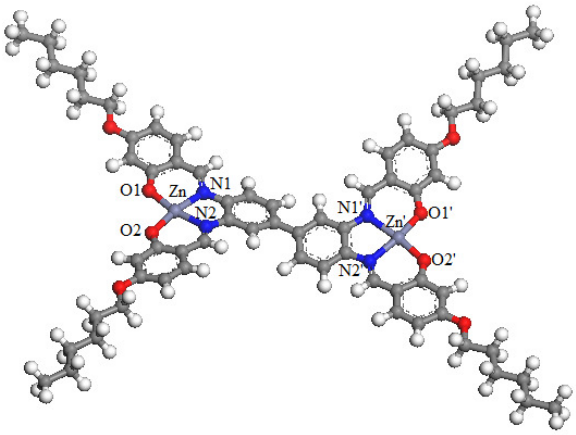

Fig. 8: Optimized structure of Zn_2-6bps.

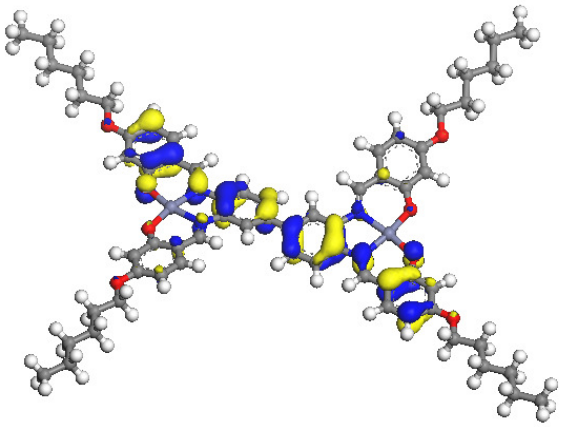

Fig. 9: HOMO of Zn_2-6bps.

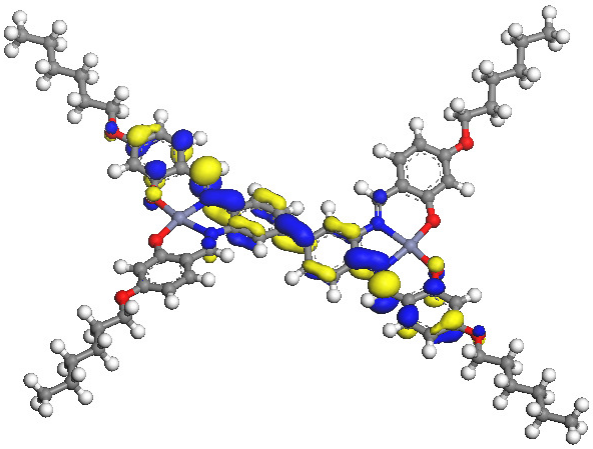

Fig. 10. LUMO of Zn_2-6bps.

Table 3: Selected bond length and bond angles of Zn_2-6bps from DFT.

Zn		**Zn′**	
Structure parameter	**Bond Lengths(Å) and Bond angles in (°)**	**Structure parameter**	**Bond Length(Å) and Bond angles in (°)**
Zn—O1	1.968	Zn′—O1	1.972
Zn—O2	1.970	Zn′—O2	1.970
Zn—N1	2.105	Zn′—N1	2.095
Zn—N2	2.098	Zn′—N2	2.102
O1—Zn—O2	97.6	O1—Zn′—O2	97.5
N1—Zn—N2	79.2	N1—Zn′—N2	79.4
O1—Zn—N1	91.5	O1—Zn′—N1	92.1
O2—Zn—N2	91.9	O2—Zn′—N2	91.8
O1—Zn—N2	169.9	O1—Zn′—N2	169.5
O2—Zn—N1	169.7	O2—Zn′—N1	169.8

5.2.2 Synthesis of dinuclear copper complexes accessed from tridentate [ONO] donor ligands:

Two new dinuclear copper(II) complexes of the type $[Cu_2(L/L^{/})_2]$ have been synthesized from the ligands [LH = (E)-5-(hexadecyloxy)-2-((2-hydroxyethylimino) methyl) phenol and $L^{/}H$ = (E)-5-(hexadecyloxy)-2-((2-hydroxypropan-2-ylimino) methyl) phenol] with slight modification of the literature procedures as presented in **Scheme 2**.

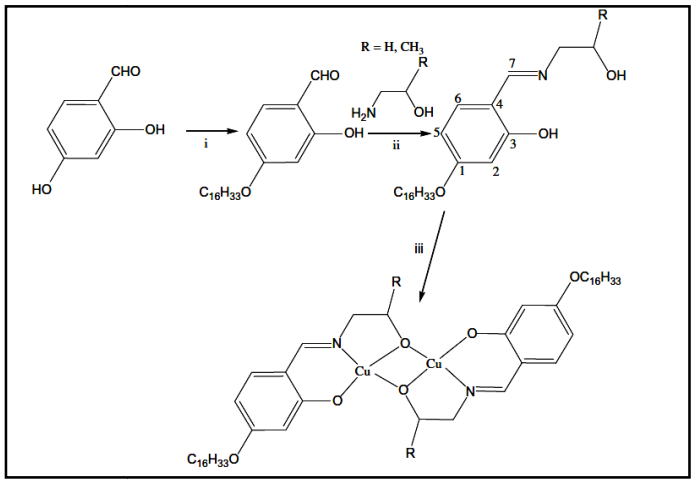

Scheme 2: i.$C_{16}H_{33}Br$, $KHCO_3$, KI, dry acetone, Δ, 40h, and ii. glacial AcOH, absolute EtOH Δ, 4h iii. $Cu(OAc)_2$. H_2O, MeOH, 1h.

Synthesis of hexadecyloxysalicyldehyde:

Alkoxysalicyldehyde derivatives were prepared following the general method reported in literature.[37] 2, 4-Dihydroxybenzaldehyde (10mmol, 1.38g), $KHCO_3$ (10mmol, 1.5g), KI (catalytic amount) and 1-bromohexadecane ($10cm^3$, 3g) were mixed in 250 cm^3 of dry acetone. The mixture was heated under reflux for 24 h, and then filtered, while hot, to remove any insoluble solids. Dilute HCl was added to neutralize the solution, which was then extracted with chloroform ($100cm^3$). The combined chloroform extract was concentrated to give a purple solid. The solid was purified by column chromatography using a mixture of chloroform and hexane (v/v, 1/1) as eluent. Evaporation of the solvents afforded a white solid product.

(E)-5-(hexadecyloxy)-2-((2-hydroxyethylimino) methyl) phenol (L):

An ethanolic solution of 2-hydroxy-(4-hexadecyloxy)-salicylaldehyde (0.36g, 1mmol) was added to an ethanol solution of 2-amino-1-ethanol (0.06g, 1mmol) The solution

mixture was refluxed with a few drops of acetic acid as catalyst for 3h to yield the yellow Schiff base. The compound was collected by filtration and recrystallised from absolute ethanol to obtain a pure compound.

Yield: 0.308g (78%) yellow colored solid; m.p. 87°C. *Anal*. Calc. for $C_{25}H_{43}NO_3$ (405.6): C, 74.06; H, 10.69; N 3.45. Found: C, 74.07; H, 10.67; N, 3.46%. ^{1}H NMR (400 MHz, $CDCl_3$): δ 0.87 (t, J=6.4Hz, -CH_3, 3H), 1.27-1.83 (m, -CH_2 of methylene proton in side chain), 3.60 (t, J=4.1Hz, -CH_2N=C, 2H), 3.73 (t, J=4.0Hz, -CH_2OH, 2H), 3.91 (t, J=8.1Hz, -OCH_2, 2H), 7.09 (d, J= 8.6Hz, -C_6H_4, 1H), 8.53 (s, -N=CH, ^{1}H), 13.8 (s,1H, OH); ^{13}C NMR (75.45 MHz; $CDCl_3$; Me_4Si at 25°C, ppm) δ= 161.3 (-C1), 101.3 (-C2), 161.9 (-C3), 116.6 (-C4), 107.3 (-C5), 132.7 (-C6), 162.1(-C7), 69.6 (-NCH_2), 68.4 (-OCH_2) FAB Mass (m/e, fragment): m/z: calc. 405.6; found: 406.6[M+H^+]; IR (ν_{max}, cm^{-1}, KBr):3433(ν_{OH}), 2918($\nu_{as(C-H),}$ CH_3), 2919($\nu_{as(C-H),}$ CH_2), 2849($\nu_{s(C-H),}$ CH_3), 2850($\nu_{as(C-H),}$ CH_2), 1626($\nu_{C=N}$), 1287(ν_{C-O}).

(E)-5-(hexadecyloxy)-2-((2-hydroxypropylimino) methyl) phenol (L$^/$):

Yield: 0.322g (75%) yellow colored solid; m.p. 88°C. *Anal*. Calc. for $C_{26}H_{45}NO_3$ (419.3): C, 74.42; H, 10.81; N 3.34. Found: C, 74.41; H, 10.83; N, 3.33%. ^{1}H NMR (400 MHz, $CDCl_3$): δ 0.89 (t, J=6.4Hz, -CH_3, 3H), 1.28 (s, -CH_3) 1.27-1.83 (m, -CH_2 of methylene proton in side chain), 3.62 (t, J=4.1Hz, -CH_2N=C, 2H), 3.74 (t, J=4.0Hz, -CH_2OH, 2H), 3.93 (t, J=8.1Hz, -OCH_2, 2H), 7.08 (d, J= 8.6Hz, -C_6H_4, 1H), 8.51(s, -N=CH, ^{1}H), 13.7 (s,1H, OH); FAB Mass (m/e, fragment): m/z: calc. 419.3; found: 420.3[M+H^+]; IR (ν_{max}, cm^{-1}, KBr):3432(ν_{OH}), 2917($\nu_{as(C-H),}$ CH_3), 2916($\nu_{as(C-H),}$ CH_2), 2845($\nu_{s(C-H),}$ CH_3), 2851($\nu_{as(C-H),}$ CH_2), 1622($\nu_{C=N}$), 1283(ν_{C-O}).

Syntheses of the copper complexes:

The ligand L (0.40g, 1mmol) or L$^/$ (0.41g, 1mmol) was dissolved in minimum volume of absolute ethanol. An equimolar amount of copper acetate $Cu(OAc)_2$. H_2O (0.19g, 1mmol) in methanol was then added slowly and stirred for 2h at room temperature. A greenish blue solid formed immediately was filtered, washed with diethyl ether and recrystallized from chloroform-ethanol (1:1).

Bis [N-(2-hydrooxyethyl)-4-hexadecyloxysalicyldiminato]copper(II) [Cu_2L_2]:

Yield=0.442g, 75%. Anal. Calc. for $C_{50}H_{82}Cu_2N_2O_6$: C, 64.28; H, 8.85; N, 3.00. Found: C, 64.27; H, 8.86; N, 3.01%. IR ($\nu_{max,}$ cm^{-1}, KBr): 2921($\nu_{as(C-H),}$ CH_3),

2851($\nu_{as(C-H),}$ CH_2), 1612($\nu_{C=N}$), 1252(ν_{C-O}, ether), 1148 (ν_{C-O}, phenolic); FAB Mass (m/e, fragment): m/z: calc. 932.4; found: 933.5[$M+H^+$].

Bis[N-(2-hydroxypropan-2-ylimino)-4-hexadecyloxysalicyldiminato]copper(II) [$Cu_2L'_2$]:

Yield=0.446g, 78%. Anal.: calc. for $C_{52}H_{86}Cu_2N_2O_6$:C, 64.90; H, 9.01; N, 2.91; found: C, 64.91; H, 9.02;N, 2.92%. IR (ν_{max}, cm^{-1}, KBr): 2922($\nu_{as(C-H),}$ CH_3), 2849($\nu_{as(C-H),}$ CH_2), 1613($\nu_{C=N}$), 1251(ν_{C-O}, ether), 1147 (ν_{C-O}, phenolic). FAB (m/e, fragment): m/z: calc.962.5; found: 963.5[$M+H^+$].

5.2.2.1 Results and Discussion:

Synthesis and structural assessment:

The Schiff base ligands were synthesized by condensation of 4-alkoxysubstituted aldehyde with a 2-amino-1-ethanol and 2-aminopropan-1-ol with slight modification of the literature procedures.[37,38] The synthetic strategy for the ligands [LH = (E)-5-(hexadecyloxy)-2-((2-hydroxyethylimino) methyl) phenol and $L'H$ = (E)-5-(hexadecyloxy)-2-((2-hydroxypropan-2-ylimino) methyl) phenol], and their bimetallic copper complexes, [$Cu_2(L/L')_2$] are presented in **Scheme 2**. Complexes formed from a reaction of appropriate ligand with copper acetate in ethanol - methanol solution in Cu: L/L' as 2:2 ratio at ambient temperature are isolated as greenish blue colored solid in good yields. The compounds were characterized by FT-IR, ^1H and ^{13}C NMR, UV-visible, elemental analyses, solution electrical conductivity measurements and FAB mass spectrometry. The CHN analyses of the ligands and their complexes are consistent with the proposed formulae, confirming the bimetallic composition of the complexes. FAB mass spectra of the compounds are concordant with their formula weights. The IR spectra of the Schiff base ligands showed a broad band in the region 3380-3366cm^{-1} attesting the presence of OH functionality. Upon complexation, this band disappears. The azomethine nitrogen $\nu_{C=N}$ stretching frequency of the free ligand appears at ~1626 cm^{-1} which gets shifted to lower wave number (~1613cm^{-1}) in the complexes indicating the involvement of azomethine nitrogen in coordination. Appearances of medium intensity bands at ~450-480cm^{-1} are attributable to ν_{Cu-N} and ν_{Cu-O}, respectively. ^1H NMR spectra of the ligands showed a broad signal at δ_H 13.4-13.8 ppm, corresponding to the phenolic proton. Appearance of sharp peak at

ca. δ_H 8.10 ppm characteristic of imine proton (H-C=N), confirmed the formation of Schiff base. The alcoholic-H appeared, expectedly, as a triplet at δ 3.74 ppm in the ligands. Owing to the paramagnetic nature of the complexes, ^{1}H NMR spectra revealed only broad unresolved signals. Solution electrical conductivity of the complexes recorded in CH_2Cl_2 (10^{-3}M) were found to be < 10 $\Omega^{-1}cm^{-1}mol^{-1}$ confirming the non-electrolytic nature of the complex.

UV-visible study:

The absorption spectra of the ligands exhibited three bands (**Fig.11**) owing to π-π* transition of the aromatic rings in the region 255-291nm. The band at 348nm is due to the π-π* transition of the C=N fragment. Upon complexation all these bands are red shifted to 279nm, 310nm and 391nm.

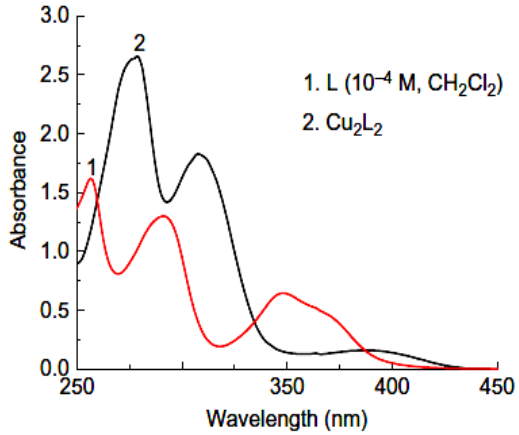

Fig. 11: UV-visible spectra of ligand and copper complex

Photoluminescence study:

Photoluminescence study of the ligands (L/L$^/$) were carried out at room temperature in dichloromethane solution and also in solid state (**Fig.12**) The ligands exhibited emission maxima at 447nm (Φ = 30%) in solution when excited at 350nm. In solid state emission maxima is red shifted to 469nm (Φ = 9%). This shift is due to the intermolecular aromatic interaction which is weaker in solution than that in the solid state.[6,37,38] Moreover in the solid state, a larger electronic delocalization leads to lowering of energy of the electronic states. Generally Schiff base systems exhibit fluorescence due to intraligand π-π* transitions.[41] Complexes did not exhibit any

fluorescence presumably because paramagnetic ions quench the fluorescence of organic ligands by enhancing the rate of non-radiative processes that compete with fluorescence.[52] It may be noted that quenching of fluorescence of a ligand by paramagnetic metal ions on complexation is a rather common phenomenon which is explained by processes such as magnetic perturbation, redox-activity, electronic energy transfer etc.[53]

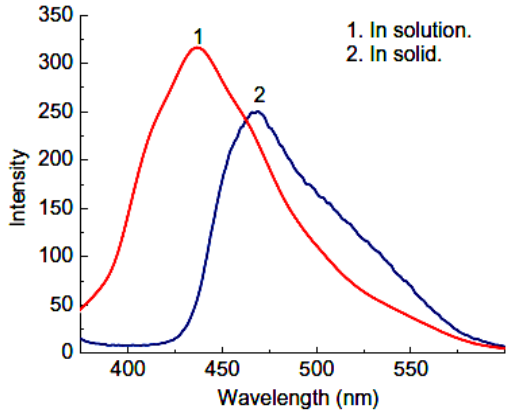

Fig. 12: Emission spectra of ligands in solution and solid state.

Mesomorphic behaviour: POM and DSC Study:

The mesomorphic behaviour of the compounds was probed by polarized optical microscopy (POM) and differential scanning calorimetry (DSC). The ligand L showed monotropic mesomorphism. On heating, the sample transformed directly to the isotropic liquid while during cooling from isotropic liquid, it first showed batonnets texture which coalesce to a high birefringent fanlike texture (**Fig.13**) at 75°C. On further cooling it solidified at 60°C. The mesophase was identified as SmA phase on the basis of these diagnostic features. The DSC trace for the compound L also showed one transition in heating cycle and two in the cooling run (**Fig.14**). The transitions at 75.1°C (ΔH = 1.9 kJmol^{-1}) is due to the change from isotropic to SmA phase. The presence of the alcoholic -OH group tends to induce attractive intermolecular interactions via H-bond (HO… HO...) resulting in liquid crystalline behaviour. Quite surprisingly, incorporation of a methyl group in amine moiety of this ligand ($L^{/}$) upsets the mesomorphism. This is ascribed to the steric hindrance caused by the tetrahedral methyl group, which resulted in loss of mesomorphism. The

complexes, however, all exhibited enantiotropic smectic mesomorphism. A typical broken focal conic-shaped texture (**Fig.15**) with homeotropic domain was observed at 114°C upon slow cooling from their isotropic liquid. The mesophase was identified as a SmA based on optical texture. DSC thermogram (**Fig.16**) showed two endothermic peaks in heating cycle and two exothermic peaks in cooling cycle. The peak at ~114-118°C is due to the I-SmA phase transition. Owing to the high viscous nature of the complexes and severe restriction in the molecular mobility, a pronounced hysteresis in transition temperature has been noted. The reversible thermal behaviour of the complexes was confirmed by DSC on subsequent heating-cooling runs. Thermal data are summarized in Table 4. Pertinent here is to mention that the structurally similar bimetallomesogens containing copper(II) ions [bis[N-(3-hydroxypropyl)-4-octanoylsalicylaldiminato] copper(II) complex reported earlier showed monotropic SmA mesophase.[10] Further, Rezvani *et al.* reported a similar bimetallic Cu(II) complexes bearing azo-linkange at the side aromatic ring showed SmA phase.[11]

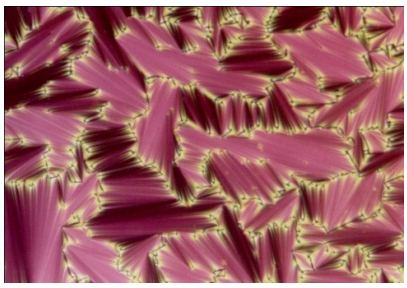

Fig. 13: Fanlike texture of SmA phase at 75°C.

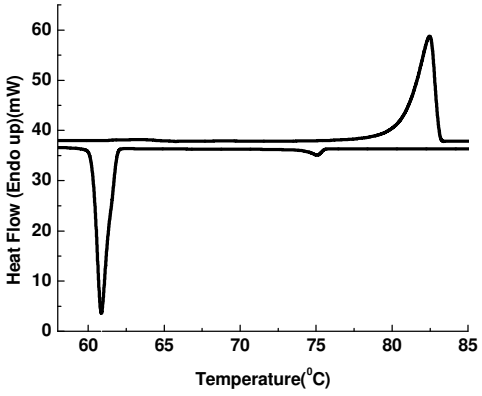

Fig. 14: DSC thermogram of L

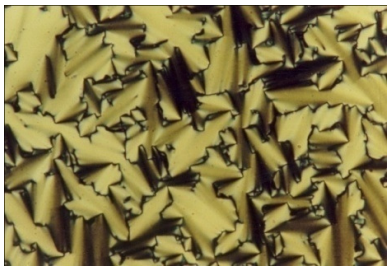

Fig. 15: Broken focal conic-shaped texture of SmA at 114°C.

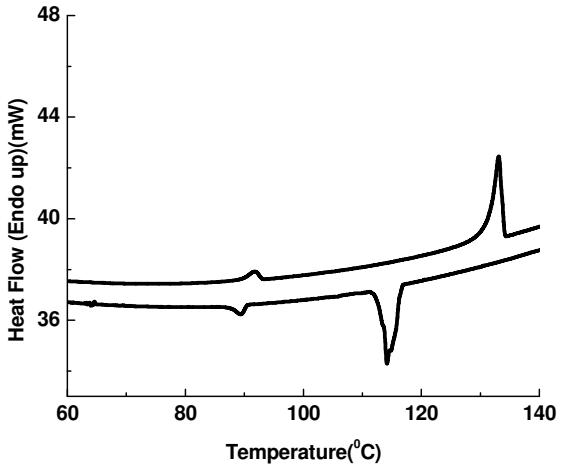

Fig. 16: DSC thermogram of Cu_2L_2.

Table 4: Mesophase transition temperatures (T°C) and associated enthalpies (ΔH, kJ mol^{-1}) of compounds.

Compounds	Heating	Cooling
L	Cr 82.4(65)I	I 75.1(1.9)SmA60.8(60.7)Cr
$L^{/}$	Cr 84.7(61.3)I	I 65.4 (59.8)Cr
Cu_2L_2	Cr 91.7(3.0)SmA133.0(27.5)I	I114.1(27.9)SmA89.3(2.6)Cr
$Cu_2L^{/}_2$	Cr 63.5(2.1)SmA136.2(47.4)I	I118.9(47.3)SmA63.5(2.3)Cr

DFT Study:

As efforts to obtain single crystal of the complexes failed, density functional theory (DFT) calculation is performed to investigate the electronic structure of the copper(II) complexes (**Fig.17** and **Fig.18**). Full geometry optimization of the complexes without

symmetry constrain has been carried out with DMol3 program package[49] using Kohn–Sham Theory. The generalized gradient approximation (GGA) was used in the calculations. At the GGA level, we have chosen the BLYP (Beck-Lee-Yang-Parr) functional which incorporates Becke's exchange and Lee–Yang–Parr correlation.[48] The DNP (Double Numerical Polarisation) basis functions, chosen in the present study, are the double-numerical atomic orbitals augmented by polarization functions, i.e., functions with angular momentum one higher than that of the highest occupied orbital in the free atom.[54] The DNP basis set is believed to be more accurate than a Gaussian basis set 6-31G** of similar size. In our calculations, self consistent field procedures are performed with a convergence criterion of 2×10^{-5} a.u. on the total energy and 10^{-6} a.u. on electron density. Some of the significant geometric parameters of the optimized copper complexes evaluated at BLYP/DNP level are shown in Table 5. The molecular structures of the complexes are nearly flat with two copper atoms lying ~3.15Å apart. The geometry around each metal centre is slightly distorted square planar. The HOMO and LUMO energies of the complex Cu_2L_2 is calculated to be -3.502eV, -3.035eV respectively, ΔE = 0.467eV and that of $Cu_2\ L'_2$ is found to be -3.515 and -3.052, ΔE = 0.463eV.

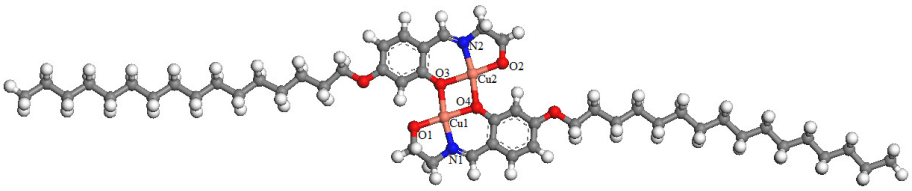

Fig. 17: Optimized structure of Cu_2L_2.

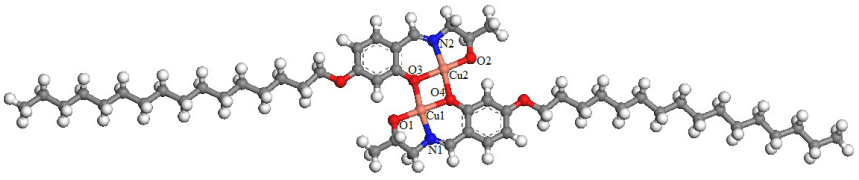

Fig. 18: **Optimized structure of $Cu_2L'_2$.**

Table 5: Selected bond length and bond angles of Cu_2 L_2 / $Cu_2L'_2$ from DFT.

	Cu_2 L_2	$Cu_2L'_2$
Structure parameter	**Bond Lengths (Å) and Bond angles in degree**	**Bond Lengths(Å) and Bond angles in degree**
Cu1—O1	1.921	1.919
Cu1—N1	1.954	1.961
Cu2—O2	1.920	1.919
Cu2—N2	1.958	1.922
Cu2—O3	2.045	2.041
Cu2—O4	2.060	2.058
Cu1 —O3	2.047	2.046
Cu1-O4	2.054	2.044
O1—Cu1—O3	103.1	103.4
O4—Cu—N1	92.0	92.0
O—Cu—O	79.5	79.6
N2—Cu2—O2	85.7	86.1
Cu1—Cu2	3.151	3.144

5.2.3 Synthesis of bimetallic zinc complex from tridentate[ONO]-donor Schiff base ligand:

The Schiff base ligand [L= (E)-5-(hexadecyloxy)-2-((2-hydroxyethylimino) methyl) phenol] and a new zinc(II) bimetallomesogenic complex, $[Zn_2L_2]$ have been synthesized following the reported method[37] as displayed in **Scheme 3**.

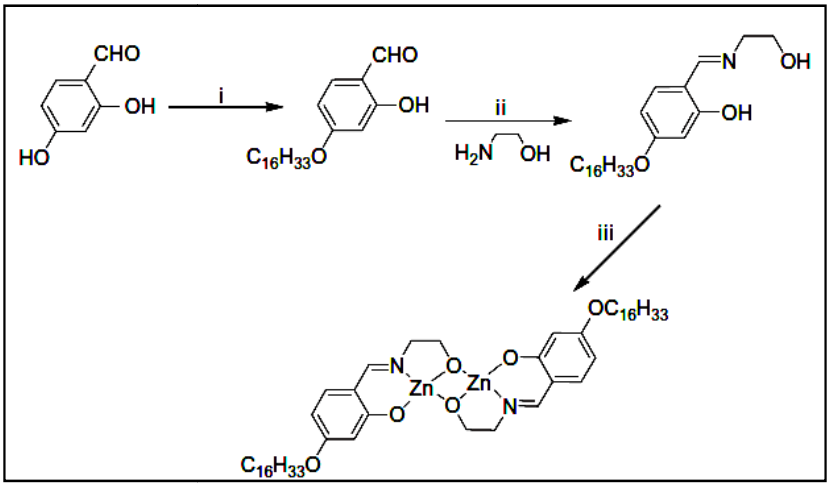

Scheme 3: i.$C_{16}H_{33}Br$, $KHCO_3$, KI, dry acetone, Δ, 40h, and ii.glacial AcOH, absolute EtOH, Δ, 4h iii. $Zn(OAc)_2.H_2O$, MeOH, stir, 6h.

Synthesis of ligand:

The synthesis and analysis of ligand (E)-5-(hexadecyloxy)-2-((2-hydroxyethylimino) methyl) phenol (L) is described in section 5.2.2.

Synthesis of zinc(II) complex:

The ligand L (0.40g, 1mmol) was dissolved in minimum volume of dry dichloromethane. To this, an equimolar amount of zinc acetate $Zn(OAc)_2.2H_2O$ (0.22g, 1mmol) in methanol was then added slowly and stirred for 6h at room temperature. A white solid formed immediately was filtered, washed with diethyl ether and recrystallized from chloroform-ethanol (1:1).

Yield: 0.45g (75%) white colored solid. *Anal*. Calc. for $C_{50}H_{82}N_2O_6Zn_2$ (936.47): C, 64.02; H, 8.81; N 2.99. Found: C, 64.07; H, 8.82; N, 2.96%. ^{1}H NMR (400 MHz, $CDCl_3$): δ 0.89 (t, J=6.4Hz, -CH_3, 3H), 1.29-1.87 (m, -CH_2 of methylene proton in side chain), 3.70 (t, J=4.1Hz, -CH_2N=C, 2H), 4.01 (t, J=8.1Hz, -OCH_2, 2H), 7.13 (d, J= 8.4Hz, -C_6H_4, 1H), 8.59 (s, -N=CH, ^{1}H). FAB Mass (m/e, fragment): m/z: calc. 936.47; found: 937.47[M+H$^+$]; IR (ν_{max}, cm^{-1}, KBr): 2922($\nu_{as(C-H),}$ CH_3), 2824($\nu_{s(C-H)}$, CH_3), 1612($\nu_{C=N}$), 1287(ν_{C-O}), 535 (ν_{M-N}), 486(ν_{M-O}).

5.2.3.1 Results and discussion:

Synthesis and structural assessment:

The Schiff base ligand [L= (E)-5-(hexadecyloxy)-2-((2-hydroxyethylimino) methyl) phenol] has been synthesized following the reported method,[37] described in section 5.2.2. The reaction of the ligand with an equimolar amount of zinc acetate in dichloromethane/methanol mixture under stirring condition leads to the formation of white solid product of Zn_2L_2 in good yield (**Scheme 3**). The ligand to metal (1:1) stoichiometric ratio, purity of the compounds was confirmed by elemental analysis, IR, ^{1}H NMR and ^{13}C NMR spectroscopy. In particular, evidence for coordination of the Schiff base ligand to the Zn(II) ion was obtained from the IR spectrum by the disappearance of the OH signal and shift of the -CN stretching band to lower wave number (1612cm^{-1}) relative to the free ligand. The absence of -OH signal in the ^{1}H NMR spectrum and the upfield shift of the iminic hydrogen signal lend further credence to the coordination of the Schiff base ligand.

UV-Visible study:

The absorption spectra of Schiff base ligand and its zinc complex were recorded at room temperature (298K) in dichloromethane solvent (**Fig.19**). The electronic spectrum of the ligand showed two strong bands one at ~280 nm owing to the π-π*

transitions of the aromatic ring and another at ~308nm due to the π-π* transition of the C=N fragment. The complex showed four bands at ~289nm, ~292nm, ~297nm and ~350nm, respectively which may have arisen from metal perturbed ligand centred transition.

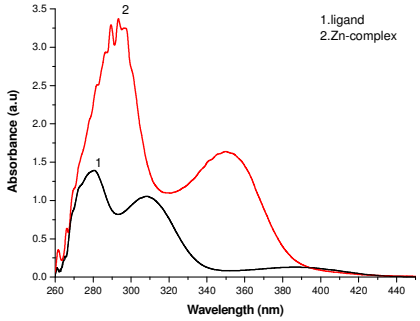

Fig.19: UV-visible spectra of the ligand and complex

Photoluminescence Study:

The ligands exhibited emission maxima at ~422nm (Φ = 15%) in dichloromethane solution when excited at 300nm (**Fig.20**). The complex is found to be emissive in solution, solid as well as in mesomorphic state. The luminescence spectrum in the solid state was recorded by placing the compound in between two quartz plates. The emission maxima (**Fig.21**) is red shifted from solution (420nm, Φ = 15%) to mesomorphic state (432nm, Φ = 7%) and to the solid state (464nm, Φ = 11%). The presence of stronger aggregation tendency in solid or mesomorphic state gives rise to a larger electronic delocalization, resulting in an energy lowering of the electronic states.

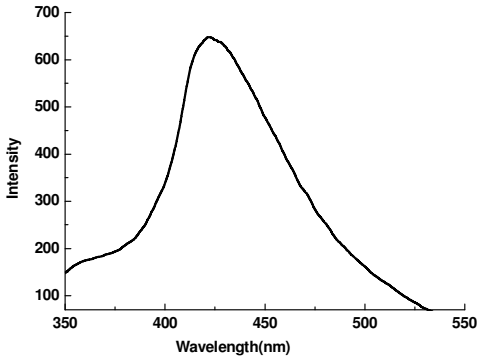

Fig.20: Photoluminescence spectrum of ligand

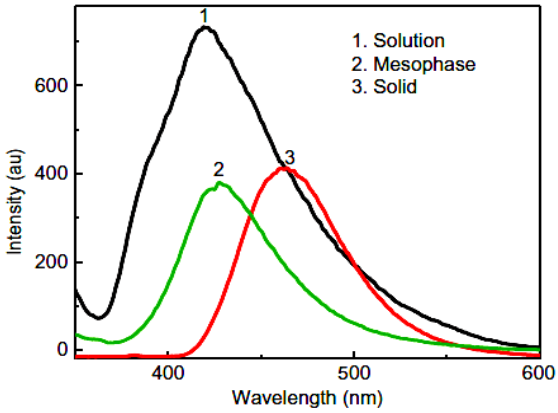

Fig. 21: Photoluminescence spectra of zinc complex

Polarising Optical microscopy and Differential Scanning Calorimetric Study:

The detail mesomorphic behaviour of the ligand and zinc complex was ascertained by POM and DSC study. The ligand showed monotropic SmA phase. The phase structures associated with the mesomorphic transitions of the ligand is described in section 5.2.2.1. Quite interestingly, the complex showed enantiotropic columnar phase. During slow cooling of the zinc complex from clearing point, a spherulitic growth appeared from dark background of isotropic melt which coalesce to a fan-like texture (**Fig.22**) at ~130.8°C revealing a typical columnar mesophase. DSC thermogram (**Fig.23**) for zinc complex exhibits three endothermic peaks and two exothermic peaks. A crystal to crystal transition was observed in DSC, thermal microscopy did not show any such transition. A very low enthalpy value (Table 6) for columnar to isotropisation and vice versa were noted for the complex.

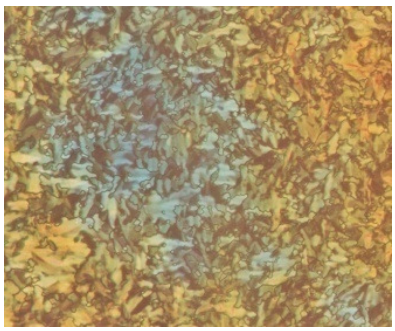

Fig. 22: POM texture of zinc complex

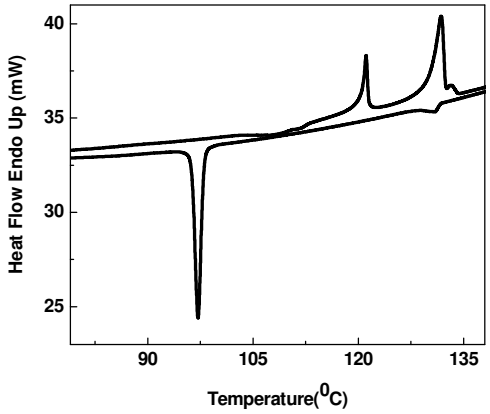

Fig. 23: DSC thermogram of zinc complex.

Table 6: Thermal data of the Zn_2L_2 complex.

Compounds	***T*** **(°C)** [a]	**Transition**[b]	**Δ*H* (kJmol^{-1})**
Zn-complex	121	Cr-Cr_1(Heating)	13.3
	131.8	Cr_1-$Col_{r/o}$(Heating)	34.2
	133.3	$Col_{r/o}$-I(Heating)	1.4
	131.7	I-$Col_{r/o}$(Cooling)	1.7
	97	$Col_{r/o}$-C_r(Cooling)	90.9

[a] Temperature at onset of peak. [b] Cr: crystal, Col_r/Col_o: columnar rectangular or oblique phase.

Powder X-ray diffraction Study:

To get information on the structural aspects, PXRD measurements were carried out in the mesophase. PXRD pattern (**Fig.24**) shows intensity versus 2θ profile at T=125°C. The broad and diffuse peak in the high angle region (**inset in Fig.24**) corresponding to a spacing of 4.4Å, reflects the liquid like ordering of the molecules within the columns. In the low angle region seven sharp peaks are seen. These peaks are indexed to a columnar phase with 2D rectangular lattice, with lattice spacing being a = 43.2Å and b = 34.9Å. The data could as well be indexed to an oblique columnar phase (Col_{ob}) with a slightly better statistical error; in this case the lattice parameters remain identical to that for the rectangular lattice with tilt of columns θ = 2.5° (Table 7). Moreover, the radius of the non-discoid molecule (~27Å) smaller than both the lattice constants (a = 43.2Å and b = 34.9Å). Therefore, a criss-cross arrangement of the molecules in perpendicular fashion, one on top of other (**Fig.25**) is contemplated to form the discoid shell.[30]

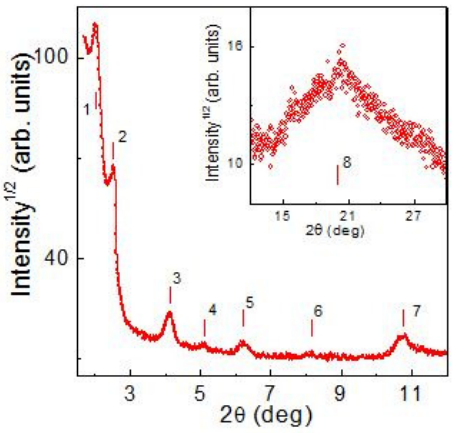

Fig. 24: X-ray diffraction pattern of Zn_2L_2 complex at 125°C.

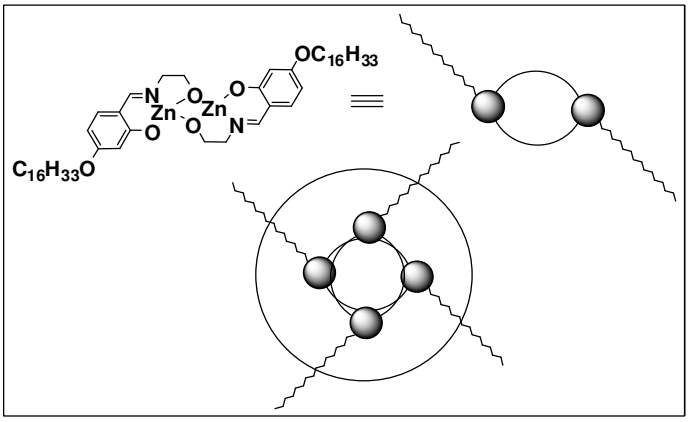

Fig. 25: Molecular organization in discoid shell.

Table 7: XRD data of the Zn_2L_2 complex

	Indexed to a rectangular lattice (Col_r)		**Indexed to a oblique lattice (Col_{ob})**	
d_{meas}	**d_{calc}**	**(hk)**	**d_{calc}**	**(hk)**
43.3	43.2	(10)	43.2	(10)
34.9	34.9	(01)	34.9	(01)
21.4	21.6	(20)	21.6	(20)
17.2	17.4	(02)	17.4	(02)
14.2	14.4	(30)	14.4	(30)
10.8	10.8	(40)	10.8	(40)
8.2	8.1	(24)	8.2	(24)
4.4				
	Cumulative error	0.161	Cumulative error	0.145
a =	43.2		a =	43.2
b =	34.9		b =	34.9
			Tilt angle θ =	2.5

Density functional and Time-dependent density functional theory study:

We have performed density functional theory (DFT) calculations to determine the electronic structure of binuclear zinc complex. Time-dependent density functional theory (TDDFT) calculations are carried out to simulate the electronic transitions observed in the experimental UV−Vis spectra.[55] Density functional theory (DFT) has become a very important tool which allows considerable insight into the electronic structures of transition metal complexes. The GAUSSIAN 09 program package[56] was employed to carry out DFT calculations at the Becke's three-parameter functional and Lee–Yang–Parr functional (B3LYP) level[48] of calculation. The 6-311G++ (d, p) basis set[57] for all atoms except for the zinc atoms which has been described by the effective core potential of Wadt and Hay (Los Alamos ECP) included in the LanL2DZ basis set was used for ground state geometry optimization and frequency calculations.[58] The gas phase ground state geometries of the binuclear zinc complex has been fully optimized using the restricted B3LYP methods without imposing any symmetry constrain with tight convergence criteria. Appropriate structure of the complex was confirmed as energy minima by calculating the vibrational frequency and confirming the absence of any imaginary frequencies. Based on the optimized geometry of the binuclear zinc complex, time dependent density functional theory (TD-DFT) calculations were performed at the B3LYP level to study the spectroscopic and electronic properties of the title complex as an isolated molecule. As the spectroscopic experiment is performed in the dichloromethane as solvent, the solvent effects have been taken into account in the theoretical calculations. A solvation method of the polarizable continuum model (PCM)[59] using the integral equation formalism variant (IEF)[60] were considered in calculations. GAUSSSUM[61] program was used to calculate the fractional contributions of various groups to each molecular orbital. Some of the important geometric parameters of the optimized binuclear zinc complex, evaluated by DFT calculation at B3LYP level are reported in Table 8. From DFT data, it is noticed that the complex has an average Zn—O and Zn—N bond lengths are in the range of 1.954–2.083 and 2.074–2.025 Å, respectively. The distance between the bridging oxygen atoms and zinc atoms are found slightly larger than the normal Zn—O bond lengths. The O1—Zn1—O3 and N1—Zn1—O2 bond angles are 147.8° and 136.6°, respectively, while, O2—Zn2—O4 and N2—Zn2—O1 bond angles are

found to be 148.3° and 136.2°, respectively. The bond angels 80.6°, 121.1°, 92.3° and 82.6° for N1—Zn1—O1, O3—Zn1—O3, N1—Zn1—O3 and O1—Zn1—O2, respectively, while, the bond angles 80.5°, 121.1°, 92.3° and 83.2° are evaluated to be for N2—Zn2—O2, O1—Zn2—O4, N2—Zn2—O4 and O1—Zn2—O2, respectively, around the zinc atoms indicating distorted square planar geometry (**Fig.26**). The dihedral angles N1—O3—O2—O1 and N2—O4—O1—O2 as computed from DFT are found to be -39.3^0 and 39.2^0, respectively (Table 8) reflecting a deviation from planarity. **Fig.27** and **Fig.28** displays the energy as well as atomic orbital composition of the highest occupied molecular orbitals (HOMO) and the lowest unoccupied molecular orbitals (LUMOs) for the zinc complex. It is noticed from **Fig.27**, HOMO of the zinc complex is composed of a mixture of 2% Zn dπ orbital and 98% pπ orbitals of the ligand. The calculated LUMO and HOMO energies are -1.33 and -5.66eV, respectively. The energy difference (ΔE) of the complex has been found to be 4.33eV mateches quite well with experimental value (~4.02eV). High LUMO–HOMO energy gap implies the stability of the complex. HOMO-1, HOMO-2, HOMO-3 and HOMO-4 orbitals in the complex have a sizeable contribution from ligand pπ orbital, while HOMO-1 and HOMO-4 have also very little contribution from metal bonding orbital (dπ) orbitals. The electron densities LUMO, LUMO+1 and LUMO+3 orbitals in the title complex are localized across the ligand $p\pi^*$ orbitals as well as zinc p orbitals. In contrast, LUMO+2 and LUMO+4 is mainly located on the metal and the ligand pπ* orbital. TD-DFT data suggested that the HOMO of the complexes comprises of mainly by ligand pi orbital (98-100%). To explain the assignment of bands in the UV region, time dependent DFT (TD-DFT) calculations have been carried for ligand and its binuclear zinc complex. The calculated absorption bands in their ground state, their oscillator strength (*f*), energies and the band assignments are tabulated in Tables 9 and 10, respectively. The surface of each peak in the spectra is proportional to oscillator strength (*f*) and which also reveals the probability of electronic transition. The electronic excitations with the highest oscillator strengths, the orbitals involved in these transitions with the percentage of contribution to each transition are presented in Tables 9 and 10. The ligand shows two absorption bands of electronic transitions at 294 and 269nm. The band at 294nm corresponds to HOMO→LUMO electronic transition owing to the L(π) →L(π*) ,

where HOMO corresponds to π bonding orbitals of C=N bond of the ligand while LUMO corresponds to π* (anti-bonding) orbitals of the C=N (intra-ligand charge transfer). This transition is consistent with the experimental value of 308 nm. Another absorption band at 269nm corresponds to HOMO→LUMO+1 electronic transition due to the L(π) →L(π*) transition of aromatic rings in the ligand.

The lower energy absorption band of zinc complex occurs at 329nm which could be assigned to HOMO→LUMO+1 or HOMO-1→LUMO electronic transition predominantly due to an intra ligand ($\pi \rightarrow \pi^*$) charge transfer. This transition resembles the experimental value of 350nm, ε=16320 $lmol^{-1}cm^{-1}$. The absorption at 283nm region is from HOMO-2→LUMO transition is of intra ligand (π→π*) charge transfer type which is comparable with the experimental transition at 297 nm. The sharp peak at 277nm (experimental value 293nm) is caused by electron transfer from HOMO-4→LUMO+1 transition which is mainly due to M(dxy→L(π*)/L(π→π*). The relatively high energy absorption band occurring at 271nm is assigned to HOMO-3 to LUMO+1 electronic transition comparable to the experimental result of 289nm. The results indicate that the UV-absorption spectra of the ligand and the bimetallic zinc complex calculated by TD-DFT method are in good agreement with the experimental data. TD-DFT data indicates that the absorption maxima are at low energy in both ligand and complex which comprised mainly of ligand based π →π* transition with marginal contribution of metal to ligand charge transfer transition.

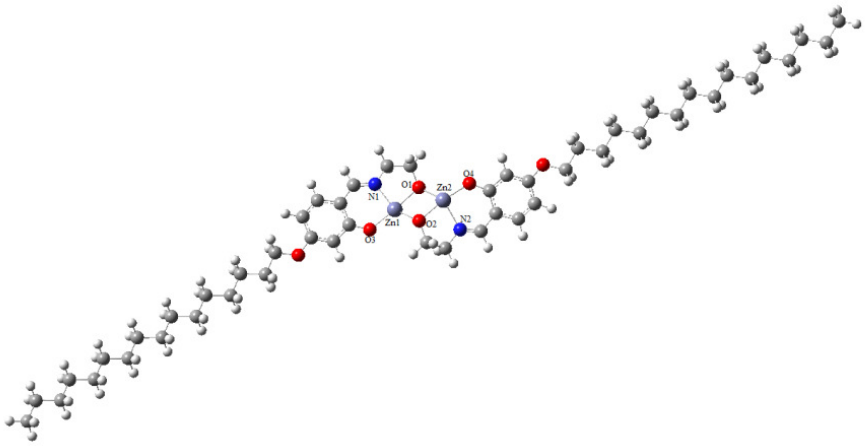

Fig. 26: Optimized structure of binuclear zinc complex

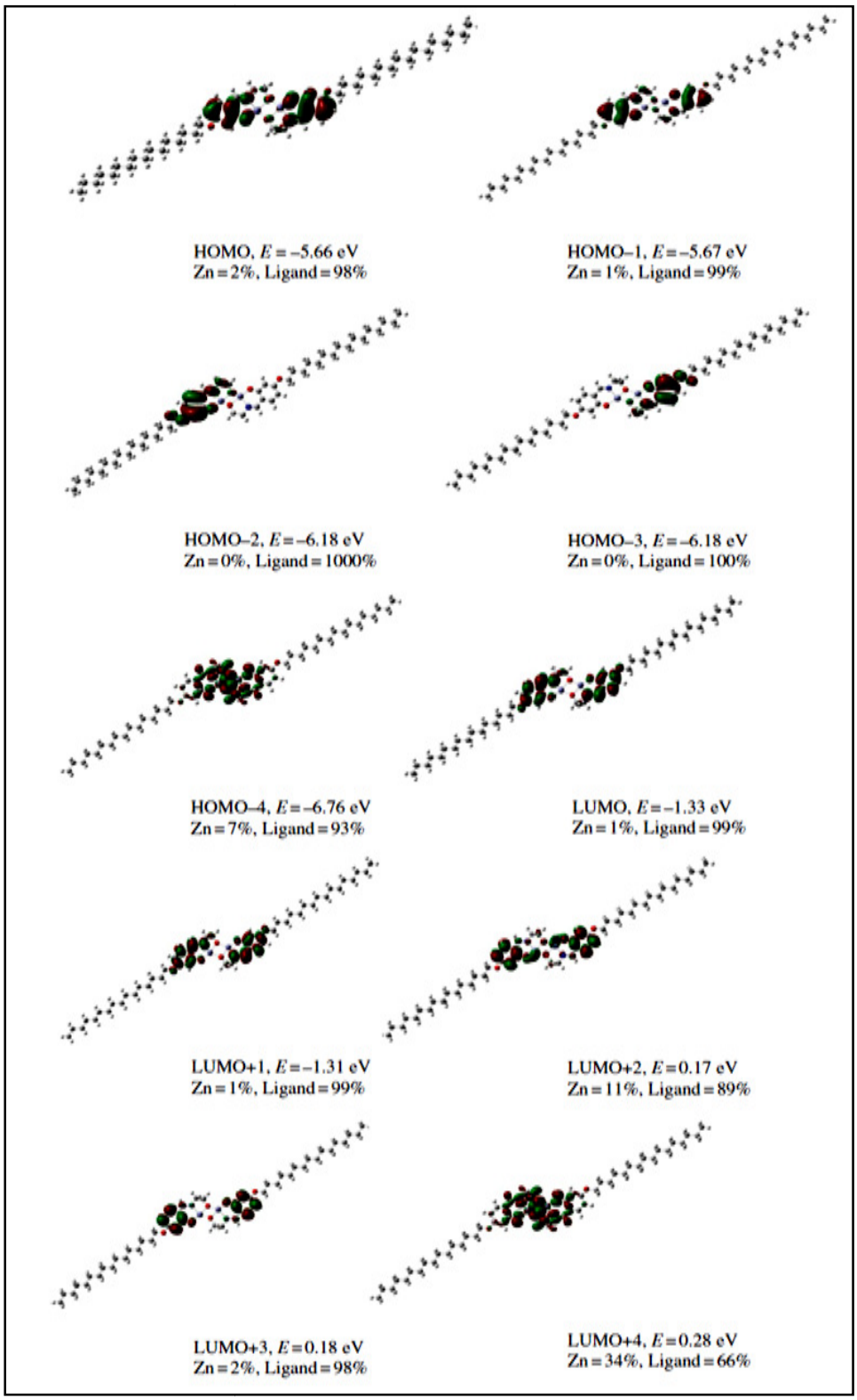

Fig. 27: Contour plots of some selected molecular orbitals.

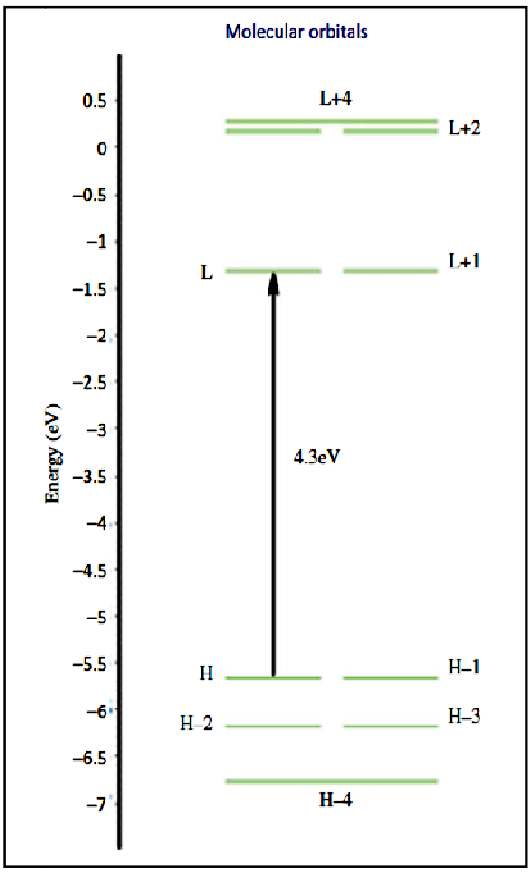

Fig. 28: Energy level diagram of MO.

Table 8: Selected bond lengths (Å) and angles (°) for the binuclear zinc complex evaluated at B3LYP level.

Structural parameter	Complex	Structural parameter	Complex
Zn1—O1	2.080	Zn2—O1	1.975
Zn1—O2	1.975	Zn2—O2	2.083
Zn1—O3	1.954	Zn2—O4	1.954
Zn1—N1	2.074	Zn2—N2	2.075
O1—Zn1—O3	147.8	O2—Zn2—O4	148.3
N1—Zn1—O2	136.6	N2—Zn2—O1	136.2
N1—Zn1—O1	80.6	N2—Zn2—O2	80.5
O2—Zn1—O3	121.1	O1—Zn2—O4	121.1
N1—Zn1—O3	92.3	N2—Zn2—O4	92.3
O1—Zn1—O2	82.6	O1—Zn2—O2	83.2
N1—O3—O2—O1	-39.3	N2—O4—O1—O2	39.2

Table 9: The experimental absorption bands and the electronic transitions calculated with TDDFT/B3LYP method for the ligand.

Key Transition	Character	λ(nm)	E(eV)	*f* Osc. strength	Assignment	λexp(nm) ε(lmol $^{-1}$cm^{-1})
(72%)HOMO→LUMO	L(π) →L(π*)	294	4.213	0.261	IL(C=N)	308/10794
(72%)HOMO→LUMO+1	L(π) →L(π*)	269	5.392	0.124	IL(aromatic ring)	280/14137

Table 10: The experimental absorption bands and the electronic transitions calculated with TDDFT/B3LYP method for binuclear zinc complex.

Key Transition	Character	λ(nm)	E(eV)	*f* Osc. strength	Assignment	λexp(nm) ε(lmol^{-1}cm^{-1})
(48%)HOMO-1→LUMO /(44%)HOMO →LUMO+1	L(π)→L(π*)/ L(π)→L(π*)	329	3.768	0.320	IL	350(16320)
(28%)HOMO-2→LUMO /(16%)HOMO-2→LUMO+1 /(15%)HOMO-3→LUMO+1	L(π)→L(π*)/ L(π)→L(π*)/ L(π)→L(π*)	283	4.381	0.816	IL	297(32739)
(26%) HOMO-4→LUMO+1 /(12%)HOMO-2→LUMO	M(d_{xy})→L(π*)/ L(π)→L(π*) L(π)→L(π*)	277	4.469	0.433	MLCT/IL	293(33604)
(50%)HOMO-3→LUMO+1 /(35%)HOMO-3→LUMO	L(π)→L(π*)/ L(π)→L(π*)	271	4.556	0.018	IL	289(32936)

5.3 Conclusion:

In this chapter synthesis of two new compartmental salen type Schiff base compounds with four terminal chains (short and long) and its binuclear zinc(II) complexes are described. The ligands besides being fluorescent exhibit monotropic nematic/SmC mesophase transition, however, the complexes lack any mesomorphism but exhibited intense fluorescence. Interestingly different chain length of alkoxy group promoted quite different mesomorphic behaviour. Based on spectral and DFT study, four

coordinate distorted square planar geometry around Zn(II) centre have been conjectured. The strategy adopted herein can be effectively employed to access a variety of newer bimetallic systems with tunable molecular construction motifs leading to smart multifunctional materials. An attractive option would be to access paramagnetic photoluminescent bimetallomesogens.

Two new tridentate [ONO]-donor one-ring Schiff base ligands with substituted long alkoxy group and their dinuclear copper(II) complexes have been synthesised and their mesomorphic and photophysical properties investigated. The ligands are found to be intense blue light emitters, showing emission maxima in the range ~447-469nm both in solution and in the solid state. Interestingly, the steric constraints imposed by the methyl group in the spacer of the Schiff base ligand are speculated to have upset the mesogenicity; however, in the absence of the methyl group, liquid crystallinity could be observed. Lower conductivity values confirm the non-electrolytic nature of the complexes. Thermally very stable, the complexes exhibited a fanlike textural pattern characteristic of the enantiotropic SmA mesophase. Based on the spectral and density functional theory (DMol3) study, a distorted square planar geometry around each metal centre in the dinuclear framework has been conjectured. The synthetic strategy employed may be profitably utilised to access dinuclear complexes of different metals.

A novel bimetallic zinc complex has been prepared. Quite interestingly the complex is found to be mesogenic as well as luminescent. The complex exhibit blue emission in solid, solution as well as in mesomorphic state. A rectangular (/oblique) columnar mesomorphism induced in the complex is evident from the POM, DSC and PXRD measurements. The complex reported here is believed to be the first example of edge shared bimetallic zinc complex that showed columnar mesophase. A criss-cross arrangement of one molecule on top of the other with the flexible alkoxy arms spread out at 90° apart relative to each other has been proposed to explain their discotic character. A distorted square planar geometry is conjectured on the basis of DFT study. TD-DFT computed electronic transition data matches well with the experimental results. The synthetic strategy may serve as paradigm to access multifunctional bimetallic complexes utilising tridentate donors.

References:

1. Donnio, B.; Guillon, D.; Deschenaux, R.; Bruce, D. W. *Comprehensive Coordination Chemistry II*; Elsevier: Oxford, **2003**, *7*, 357.
2. Coe, B. J. *Comprehensive Coordination Chemistry II*; Elsevier Pergamon: Oxford, **2004**, *9*, 621.
3. Hoshino, N. *Coord. Chem. Rev.* **1998**, *174*, 77.
4. Giroud-Godquin, A. M.; Maitlis, P. M. *Angew. Chem., Int. Ed.* **1991**, *30*, 375.
5. Espinet, P. M.; Esteruelas, A.; Oro, L. A.; Serrano, J. L.; Sola, E. *Coord. Chem. Rev.* **1992**, *117*, 215.
6. Pucci, D.; Aiello, I.; Bellusci, A.; Crispini, A.; Ghedini, M.; La Deda, M. *Eur. J. Inorg. Chem.* **2009**, 4274.
7. Chakraborty, S.; Laye, R. H.; Paul, R. L.; Gonnade, R.; Puranik, V. G.; Ward, M. D.; Lahiri, G. K. *J. Chem. Soc., Dalton Trans.* **2002**, 1172.
8. Erxleber, A.; Hermann, J. *J. Chem. Soc., Dalton Trans.* **2000**, 569.
9. Wang, W. H.; Jin, G. X. *Inorg. Chem. Commun.* **2006**, *9*, 548.
10. Lai, C. K.; Leu, Y. F. *Liq. Cryst.* **1998**, *25*, 689.
11. Rezvani, Z.; Ghanea, M. A.; Nejati, K.; Baghaei, S. A. *Polyhedron* **2009**, *28*, 2913.
12. Espinet, P.; Hernandez, C.; M-Alvarez, J. M.; Miguel, J. A. *Inorg. Chem.* **2004**, *43*, 843.
13. Lai, C.K.; Lin, R.; Lu, M. Y.; Kao, K. C. *J. Chem. Soc., Dalton. Trans.* **1998**, 1857.
14. Ku, S. M.; Wu, C. Yi.; Lai, C. K. *J. Chem. Soc., Dalton. Trans.* **2000**, 3491.
15. Li, S.Y.; Chen, C. J.; Lo, P. Y.; Sheu, H. S.; Lee, G. H.; Lai, C. K. *Tetrahedron* **2010**, *66*, 6101.
16. Barbera, J.; Gimenez, R.; Marcos, M.; Serrano, J. L.; Alonso, P. J.; Martinez, J. I. *Chem. Mater.* **2003**, *15*, 958.
17. Chae, H. W.; Kadkin, O. N.; Choi, M. G. *Liq. Cryst.***2009**, *36*, 53.
18. Marcos, M.; Omenat, A.; Barbera, J.; Duran, F.; Serrano, J. L. *J. Mater. Chem.* **2004**, *14*, 3321.
19. Lai, C. K.; Serrette, A. G.; Swager, T. M. *J. Am. Chem.Soc.* **1992**, *114*, 7948.

20. Espinet, P.; Lalinde, E.; Marcos, M. Perez, J.; Serrano, J. L. *Organometallics* **1990**, *9*, 555.
21. Eguchia, S.; Nozaki, T.; Miyasaka, H.; Matsumoto, N.; Okawa, H.; Kohata, S.; H-Miyajima, N. *J. Chem. Soc., Dalton Trans.* **1996**, 1761.
22. Ghedini, M.; Pucci, D.; Munno, G. D.; Viterbo, D.; Neve, F.; Armentano, S. *Chem. Mater.* **1991**, *3*, 65.
23. Lai, C.K.; Chang, C. H.; Tsai, C. H. *J. Mater. Chem.* **2007**, *17*, 2319.
24. Glebowska, A.; Przybylski, P.; Winek, M.; Krzyczkowaska, P.; Krowczynski, A.; Szydlowska, Z.; Pociecha, D.; Gorecka, E. *J. Mater. Chem.* **2009**, *19*, 1395.
25. Barbera, J.; Levelut, A.M.; Marcos, M.; Romero, P.; Serrano, J. L. *Liq. Cryst.* **1991**, *10*, 119.
26. Barbera, J.; Gimenez, R.; Gimeno, N.; Marcos, M.; Pina, M. D. C.; Serrano, J. L. *Liq. Cryst.* **2003**, *30*, 651.
27. Bushby, R. J.; Lozman, O. R.; *Curr. Opin. Coll. Interface Sci.* **2002**, *7*, 343.
28. Neill, O. M.; Kelly, S. M. *Adv. Mater.* **2003**, *15*, 1135.
29. Hanna, *J. Opto-Electron Rev*. **2005**, *13*, 259.
30. Ghedini, M.; Pucci, D.; Crispini, A.; Bellusci, A.; Deda, M. L.; Aiello, I.; Pugliese, T. *Inorg. Chem. Commun.* **2007**, *10*, 243.
31. Cavero, E.; Uriel, S.; Romero, P.; Serrano, J. L.; Gimenez, R. *J. Am. Chem. Soc.* **2007**, *129*, 11608.
32. Dambal, H. K.; Yelamaggad, C. V. *Tet Lett.* **2012**, *53*, 186.
33. Cozzi, P. G.; Dolci, L. S.; Garelli, A.; Montalti, M.; Pordi, L.; Zaccheroni, N. *New J. Chem.* **2003**, *27*, 692.
34. Splan, K. E.; Massari, A. M.; Morris, G. A.; Sun, S. S.; Reina, E.; Nguyen, S. B. T.; Hupp, J. T. *Eur. J. Inorg. Chem.* **2003**, 2348.
35. Xing, L.; Zha, M.-Q.; Lu, Y.; Bing, Y.; Zhu, C.-F.; Cui, Y. *Synth. React. Inorg. Met. Org. Nano Met. Chem.* **2010**, *40*, 451.
36. Liuzzo, V.; Oberhauser, W.; Pucci, A. *Inorg. Chem. Commun.* **2010**, *13*, 686.
37. Bhattacharjee, C. R.; Das, G.; Mondal, P.; Rao, N. V. S. *Polyhedron* **2010**, 29, 3089.

38. Bhattacharjee, C. R.; Das, G.; Mondal, P.; Prasad, S. K.; Rao, D. S. S. *Eur. J. Inorg. Chem.* **2011**, 1418.
39. Bagherzadeh, M.; Amini, M. *J. Coord. Chem.* **2010**, 10, 3849.
40. Geary, W. *J. Coord. Chem. Rev.* **1971**, *7*, 81.
41. Chattopadhyay, T.; Mukherjee, M.; Banu, K.S.; Banerjee, A.; Suresh, E.; Zangrando, E.; Das, D. *J. Coord. Chem.* **2009**, *62,* 967.
42. Roy, P.; Dhara, K.; Manassero, M.; Ratha, J.; Banerjee, P. *Inorg. Chem.* **2009**, *46*, 6405.
43. Dollberg, C. L.; Turro, C. *Inorg. Chem.* **2001**, *40*, 2484.
44. Roundhill, D. M., Modern Inorganic Chemistry Series; in: J.P. Fackler (Ed.), Plenum Press: New York, **1994**.
45. Hung, S. F.; Ling, X. H.; Fang, H. C., Zhan, X. L.; Zhou, Z. Y.; Chen, L.; Cai, X. P. *Transition Met. Chem.* **2009**, *34,* 115.
46. Venkatachalam, G.; Raja, N.; Pandiarajan, D.; Ramesh, R. *Spectrochim. Acta Part A* **2008**, *71*, 884.
47. Patel, D. B.; Bhattacharya, P. K. *Mol. Cryst. Liq. Cryst.* **2005**, *432*, 47.
48. Lee, C.; Yang, W.; Parr, R.G. *Phys. Rev. B* **1988**, *37*, 785.
49. Delley, B. J. *Chem. Phys.* **1990**, *92*, 508.
50. Gordon, M. S. *Chem. Phys. Lett.* **1980**, *76*, 163.
51. Lin, H. C.; Huang, C. C.; Shi, C. H.; Liao, Y. H.; Chen, C. C.; Lin, Y. C.; Liu, Y. H. *Dalton Trans.* **2007**, 781.
52. Chen, X.; Yamaguchi, A.; Namekawa, M.; Kamijo, T.; Teramae, N.; Tong, A. *Ana. Chim. Acta.* **2011**, *696*, 94.
53. Lu, Y.; Liu, J.W. *J. Am. Chem. Soc*. **2007**, *129*, 9838.
54. Douglas, M.; Kroll, N.M. *Ann. Phys.* **1974**, *82*, 89.
55. Holland, J. P.; Green, J. C. *J. Comput. Chem.* **2010**, *31*, 1008.
56. Frisch, M. J.; Trucks, G. W.; Schlegel, H. B.; Scuseria, G. E.; Robb, M. A.; Cheeseman, J. R.; Scalmani, G.; Barone, V.; Mennucci, B.; Petersson, G. A.; Nakatsuji, H.; Caricato, M.; Li, X.; Hratchian, H. P.; Izmaylov, A. F.; Bloino, J.; Zheng, G.; Sonnenberg, J. L.; Hada, M.; Ehara, M.; Toyota, K.; Fukuda, R.; Hasegawa, J.; Ishida, M.; Nakajima, T.; Honda, Y.; Kitao, O.; Nakai, H.; Vreven, T.; Montgomery, J. A.; Peralta, J. E. Jr.; Ogliaro, F.; Bearpark, M.;

Heyd, J. J.; Brothers, E.; Kudin, K. N.; Staroverov, V. N.; Kobayashi, R.; Normand, J.; Raghavachari, K.; Rendell, A.; Burant, J.C.; Iyengar, S.S.; Tomasi, J.; Cossi, M.; Rega, N.; Millam, J. M.; Klene, M.; Knox, J.E.; Cross, J. B.; Bakken, V.; Adamo, C.; Jaramillo, J.; Gomperts, R.; Stratmann, R. E.; Yazyev, O.; Austin, A. J.; Cammi, R.; Pomelli, C.; Ochterski, J. W.; Martin, R. L.; Morokuma, K.; Zakrzewski, V. G.; Voth, G. A.; Salvador, P.; Dannenberg, J. J.; Dapprich, S.; Daniels, A. D.; Farkas, O.; Foresman, J. B.; Ortiz, J. V.; Cioslowski, J.; Fox, D. J. *Gaussian 09,* Gaussian, Inc.: Wallingford, CT, **2009**.

57. Hariharan, P.C.; Pople, J.A. *Theor. Chim. Acta.* **1973**, *28*, 213.
58. Hay, P. J.; Wadt, W. R. *J. Chem. Phys.* **1985**, *82*, 270.
59. Cance, E.; Mennucci, B.; Tomasi, J. *J. Chem. Phys.* **1997**,*107*, 3032.
60. Miertus, S.; Scrocco, E.; Tomasi, J. *J. Chem. Phys.* **1981**, *55*, 117.
61. O'Boyle, N. M.; Tenderholt, A. L.; Langner, K. M. *J. Comput. Chem.* **2008**, *29*, 839.